Migration and fragmentation of invasion percolation clusters in two-dimensional porous media

Aleksandar Birovljev, Geri Wagner, Paul Meakin, Jens Feder, and Torstein Jøssang
Department of Physics, University of Oslo, P.O. Box 1048, Blindern, N-0316 Oslo, Norway
(Received 7 June 1994)

Experiments on and computer simulations of the migration of fractal, nonwetting fluid bubbles through a two-dimensional random porous medium saturated with wetting fluid are presented. A large invasion percolation bubble was initially formed by slow injection of a nonwetting fluid into a horizontal cell saturated with a denser wetting fluid. Slow, continuous tilting of the cell caused the bubbles to migrate through the medium. The interplay between local pinning forces and buoyancy led to fragmentation and coalescence of migrating bubbles. The process was simulated by a modified site-bond invasion percolation model.

PACS number(s): 47.55.Mh, 05.40.+j, 47.55.Kf, 64.60.Ak

Transport processes far from equilibrium generate complex spatial and temporal patterns. Familiar examples include convection, crack propagation, diffusion-limited aggregation, erosion, river formation, and particle deposition. In many cases, the transport process take place in disordered media and the dynamics are governed by global driving forces and local pinning forces.

In this study we are concerned with the migration of a nonwetting fluid (NWF) cluster in a random two-dimensional porous medium that is saturated with a wetting fluid (WF). The process is driven by an external force (gravity) and opposed by local pinning forces (capillarity). The structure of the original NWF cluster was destroyed in the course of the experiment, as a result of a multitude of fragmentation, migration, and coalescence events. The experiment thus allowed us to observe the fragmentation of a fractal object, a topic that has recently become the subject of growing interest [1,2].

Fluid-fluid displacement processes in porous media have been studied intensively. The process of very slow *drainage*, when a NWF displaces a WF in a porous medium, produces a structure that is well described by the *invasion percolation* (IP) model [3]. The growth of the IP cluster is governed by the local capillary forces that are related to the sizes of the pore necks in the medium. The opposite process of *imbibition* occurs when a WF displaces a NWF. Detailed studies [4–6] using micromodels of porous media and consisting of a square network of channels led to the identification of four dominant imbibition mechanisms, hereafter referred to as I1, I2, piston, and snap off. I1 denotes the imbibition of pores that are connected to remaining NWF by only one NWF pore neck. Analogously, I2 denotes the imbibition of pores connected to the remaining NWF by two NWF pore necks forming a right angle. The piston denotes the imbibition of pore necks at the NWF-WF interface, and snap off denotes the imbibition of pore necks that connect two collinear NWF pores. Both the I2 and piston may lead to fragmentation of the structure formed by the NWF.

The effects of external forces, such as gravity, on the IP process have been studied theoretically, experimentally, and through computer simulations in two and three dimensions [7–9]. These studies were concerned with gravity-stabilized displacements (less dense fluid on top). Gravity-destabilized drainage was recently studied experimentally [10], theoretically [11], and through simulations [11].

In our experiments, the two-dimensional medium consisted of a monolayer of 1 mm diameter glass beads. The beads were randomly thrown onto a sheet of sticky contact paper bounded by a rectangular silicone border until no place for additional beads remained. After removal of the excess beads, another sheet of contact paper was applied on top, to make the model air tight. The two-dimensional bead models with approximately 140×280 or 280×560 pores were sandwiched between two 25 mm thick polymethylmethacrylate plates. Inlet and outlet holes were drilled in one of the plates. The other plate had a transparent membrane attached to it which, when inflated, pressed the beads against the other plate. This ensured that the cell was only one bead thick, everywhere. The model was placed on a stand that allowed the angle of inclination θ between the plane of the model and the horizontal to be controlled.

The experimental cell was evacuated and saturated with a glycerol-water mixture with a viscosity of $\mu = 6\times10^{-2}$ P, density $\rho = 1123$ kg/m^3, and surface tension $\sigma = 64\times10^{-3}$ N/m, dyed with 1% black Nigrosine. The cell was positioned horizontally, while another, less dense fluid (air) was slowly injected through a hole in the middle of the cell until an IP cluster was formed that was as large as possible, without touching the boundaries of the cell. The IP cluster was interspersed with numerous water-filled pores and pore necks that could be engulfed by air ("trapped") or could be parts of thin "fjords" penetrating the interior of the cluster from its perimeter. The WF connectivity in such chains of nearest neighbor pore necks was maintained through WF "films" in the spaces between the glass beads and the contact paper.

When the IP cluster had reached a sufficiently large size (approximately 2000 to 7000 pores), the air injection was terminated and the cell was sealed. The cell was rotated about the horizontal axis with a constant low

velocity of 4° per hour. This corresponded to a continuous increase of the Bond number, $\mathrm{Bo} = (\Delta\rho g a^2/\sigma)\sin\theta$, which is the ratio between buoyancy and capillary forces. Here, $\Delta\rho$ is the density difference between the two fluids, g the acceleration due to gravity, and a the grain size in the medium. Under the influence of the buoyancy the IP cluster migrated and fragmented, as shown in Figs. 1(a)–1(c). The process was recorded using a Nikon camera. The negatives were digitized [9] using a Nikon 35 mm film scanner connected to an Apollo 4000 workstation.

The migration of the IP cluster started when a sufficiently large inclination angle θ was reached. The migration occurred through a sequence of steps consisting of drainage events at the upper front and imbibition events at the lower front of the migrating cluster. An elongated branchlike structure was formed. As the angle of inclination θ increased, the primary branch fragmented, forming the next generation of small IP-like fragments that could become mobilized at some larger θ. Since the fragmentation reduced the typical size of the NWF clusters, the buoyancy drive became insufficient for further migration and long periods of stagnation occurred. The branches meandered along the direction of the component of gravity in the plane of the cell (y direction). The branches propagated at a rate faster than the very slow rate used for IP cluster growth, but new pores were still invaded sequentially. θ was increased so slowly that the relaxation time (the time during which migration, fragmentation and coalescence occur) was much smaller than the duration of the experiment. The total volume of the NWF was conserved.

A NWF cluster with a length l_y in the y direction experiences a hydrostatic potential difference $\Delta P_g = \Delta\rho g l_y \sin\theta$ from its upper to its lower front. The cluster starts to migrate when ΔP_g exceeds the capillary pressure $p_c \sim \sigma/a$ at its upper front. Comparing these two pressures leads to $l_y \sim \mathrm{Bo}^{-1}$. During migration, the clusters become elongated in the y direction until fragmentation occurs. A rough estimate of the typical length of the newly formed fragments is provided by a similar scaling relation, $l'_y \sim \mathrm{Bo}^{-1}$, since the imbibition processes leading to fragmentation are also governed by a competition between capillary and buoyancy forces. This suggests the following simple picture: The set of NWF clusters that is present at a given moment consists of fragments that have been formed at different angles of inclination θ (or values of Bo). Fragments that are formed at θ_1 remain immobile for a while and become mobilized at θ_2, given by $l'_y(\theta_1) \simeq l_y(\theta_2)$.

From earlier theoretical and experimental work on invasion percolation in a gradient [7,10,11], it is known that the correlation length ξ scales as $\xi \sim \mathrm{Bo}^{-\nu/(\nu+1)}$, where $\nu = 4/3$. For IP branches formed by destabilized displacement, ξ measures the mean transverse width. In the absence of fragmentation, a migrating cluster is expected to match this scaling relation by dynamically adjusting its shape. Fragmentation interrupts the process of adjustment and prevents the direct observation of ξ.

The experimental process was simulated by modeling the basic mechanisms of drainage and imbibition on the pore level [12]. The model was based on the gradient-invasion percolation algorithm [3,7,9], which was extended to include imbibition, fragmentation, and coalescence [13]. A square lattice of sites and bonds was used. The sites represented pores and the bonds represented pore necks. The main features of the simulation model are described below. A complete description will be given in a forthcoming publication [14].

At the beginning of each simulation, every site was assigned a random number p' uniformly distributed from 0 to 1, and every bond was assigned a random number p (see Fig. 2). The distribution $\mathcal{P}(p)$ ranged from 0 to 1 and was obtained using pore neck size distribution data from a section of the experimental cell. The sets of random numbers $\{p\}$ and $\{p'\}$ were used to compute invasion thresholds Π^i and "withdrawal thresholds" Π^w, respec-

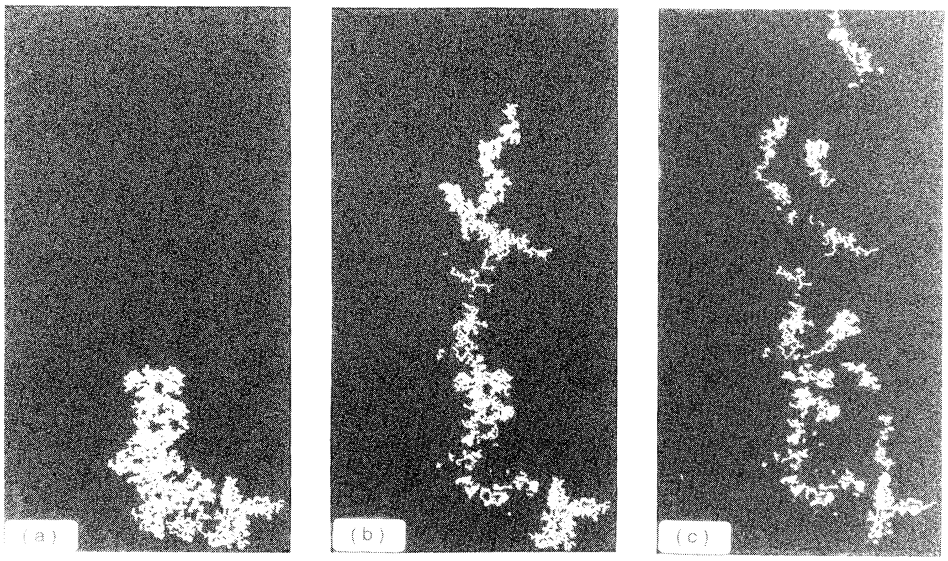

FIG. 1. (a)–(c) Pattern observed at $\theta = 0°$, 14°, and 53°, respectively. The original IP cluster shown in white covered approximately 2000 pores. (d)–(f) Simulated migrating IP clusters at $f = 0$, 0.005, and 0.013, respectively.

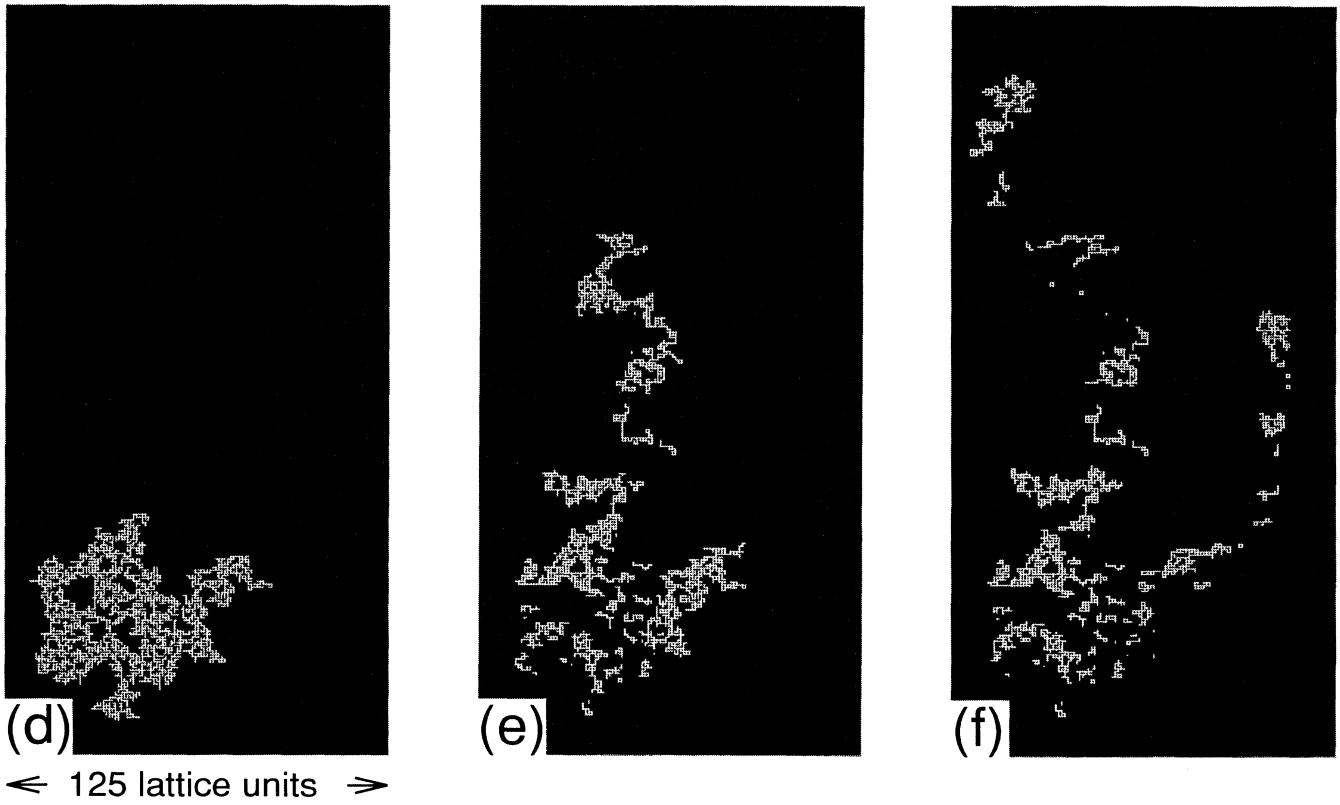

FIG. 1 *(Continued).*

tively. The results reported here were not expected to depend crucially on the exact shape of $\mathcal{P}(p)$ [11].

The simulations began by invading the center site. The standard IP algorithm with trapping [3] was applied to grow an IP cluster of a desired size, using the invasion threshold $\Pi^i = p$ for WF bonds and $\Pi^i = 0$ for WF sites, respectively. A WF site was trapped and could not be invaded if there was no path of nearest neighbor WF sites leading to the surrounding "infinite" WF cluster. A WF bond was trapped if there was no path of nearest neighbor defender bonds or sites leading to the "infinite" WF cluster.

At this stage, the buoyancy force was simulated by imposing a uniform gradient f, in the y direction, on the thresholds. The tilting of the experimental cell was simulated by increasing f by small steps. After each increment, the NWF bonds and sites were checked to determine if migration steps were possible. A migration step included withdrawing a NWF source site (or bond) and invading a WF destination site (or bond). The source and the destination had to belong to the same NWF fragment. The invasion events were opposed by the invasion thresholds Π^i whereas the withdrawals were supported by withdrawal contributions Π^w. The next step was determined by finding the global minimum of

$$\Pi = \Pi^i - \Pi^w - f\Delta y \,. \tag{1}$$

The last term in Eq. (1) accounted for the driving buoyancy force given by the height difference Δy between source and destination, times the gradient f. Π^w was a simple function of the random numbers p' and the local configuration of the interface that established a hierarchy between the four imbibition mechanisms listed above. I1 withdrawal was possible for NWF sites with only one adjacent NWF bond ($\Pi^w = \frac{1}{2}p' + \frac{1}{2}$). I2 withdrawal was possible for NWF sites with two adjacent NWF bonds forming a right angle ($\Pi^w = \frac{1}{2}p'$). NWF bonds that connected a NWF site to a WF site could be withdrawn pistonlike ($\Pi^w = 1$), and NWF bonds that connected two NWF sites could be withdrawn by snap-off ($\Pi^w = 0$). I1 and piston withdrawals were favored according to these rules. I2 site withdrawal and bond withdrawal by snap-off could cause fragmentation of the original IP cluster. See Fig. 2 for an illustration.

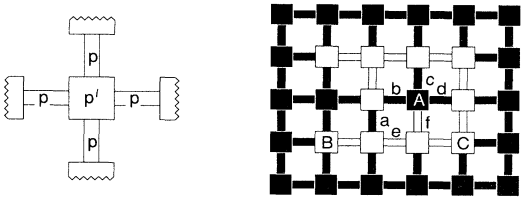

FIG. 2. Illustration of the site-bond model. To the left: bonds are assigned random numbers p and sites are assigned random numbers p'. To the right: the WF site A is trapped by the IP cluster (white). The WF bonds a, b, c, and d are not trapped. The NWF site B can be withdrawn by I1, and the site C can be withdrawn by I2 (two adjacent NWF bonds). The snap-off withdrawal of the NWF bond e would lead to fragmentation, in contrast to the pistonlike withdrawal of f.

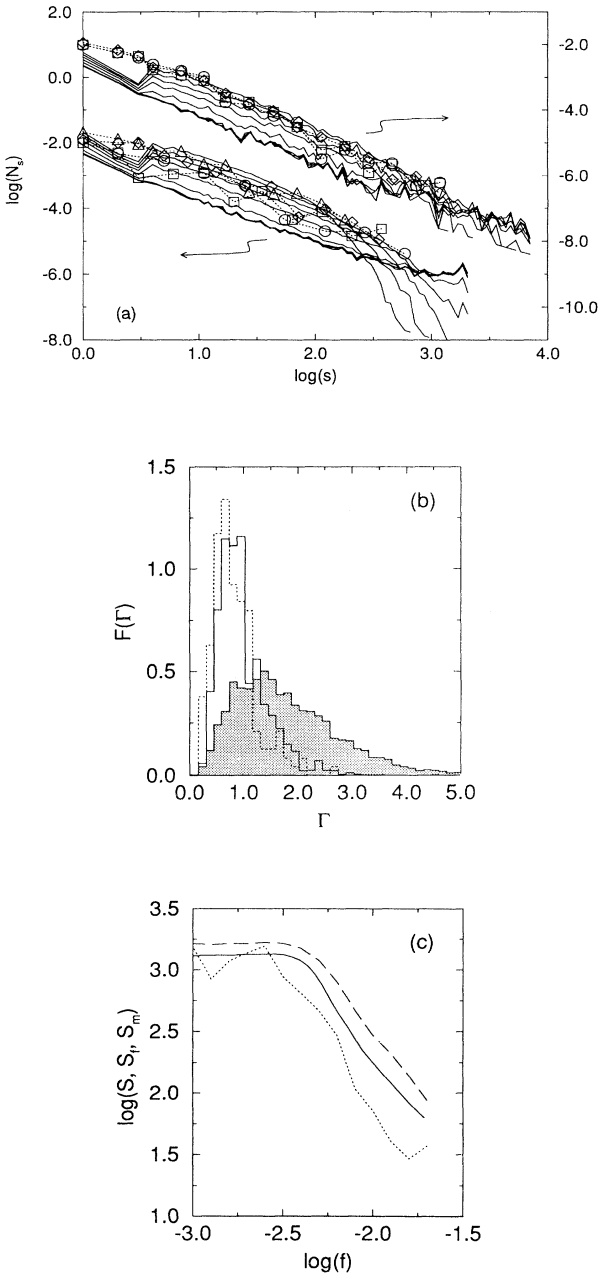

FIG. 3. (a) The number density of fragments N_s plotted as a function of size s on a log-log (base of log is 10) scale. The solid lines are simulated distributions for various values of the gradient f in which the IP clusters had a mass of 2000 (lower data set, $0 \leq f \leq 0.02$) and 7000 (upper data set, $0 \leq f \leq 0.01$). The symbols are distributions from the corresponding experiments. (b) The x/y ratio Γ of fragments observed in the experiment (dotted line) and of simulated fragments at $f = 0.005$ and $f = 0.013$ (solid line) is around 1. Just before they underwent fragmentation, fragments tended to have $\Gamma > 1$ (shaded area). (c) The simulated mean fragment size $S(f)$ (solid line) lies between the mean size $S_f(f)$ of newly formed fragments (dotted line) and the mean size $S_m(f)$ of fragments that begin to migrate (dashed line). The IP clusters had a mass of 2000.

Physically, f corresponds to the Bond number Bo used in the experiment. A quantitative mapping between f and Bo was not attempted since the distribution of the imbibition threshold pressures in the experiment was not known. In each step, incompressibility of the WF was taken into account using the same trapping rule that was used during the formation of the original IP cluster. Only steps with $\Delta y > 0$ and $\Pi < 0$ were allowed. If no possible step could be found, f was increased. Figure 1(a) shows patterns obtained in a simulation in which 2000 sites were invaded.

The distributions of the fragment sizes in both the experiments and the simulations were measured. Figure 3(a) shows the logarithmically binned fragment size distribution measured in two experiments (symbols) at several different Bond numbers and in the simulations (solid lines). About 2000 pores were invaded by NWF in one experiment (lower data set), and about 7000 in another experiment (upper data set). In the simulations IP clusters with corresponding sizes were generated on square lattices of size 200×600 and 400×2400. The gradient $|f|$ was increased in steps of $\Delta|f| = 3 \times 10^{-5}$ from 0 to 0.02 and in steps of $\Delta|f| = 1 \times 10^{-5}$ from 0 to 0.01, respectively. The simulated distributions were averaged over 1400 runs for IP clusters of size 2000 and over 70 runs for clusters of size 7000. The kink at low fragment sizes is due to the geometry of the square lattice, which made the formation of fragments of size 2 and 3 unlikely. The simulation data in the lower set show a cutoff at high fragment sizes. In the experiments, and in the upper simulation data set, the cutoff is not apparent for statistical reasons.

The immobile fragments observed in the experiment were found to have roughly the same extension in the x and y direction, in agreement with the scenario described above. Figure 3(b) shows a plot of the probability density $F(\Gamma)$, where Γ denotes the extension in the y direction divided by the extension in the x direction, and $F(\Gamma)d\Gamma$ is the probability of finding a fragment with an aspect ratio in the range Γ, $\Gamma+d\Gamma$. The histogram is based on observations at several different values of Bo. The corresponding histogram for immobile simulated fragments was measured at two values of f. The histogram for fragments that had migrated and were in the process of fragmenting [shaded in Fig. 3(b)], measured at different values of f, indicates adjustment of the fragment shape by elongation in the y direction.

Figure 3(c) shows that the simulated mean fragment size $S(f)$ (measured when all migration had ceased) decreases with increasing gradient. S is bounded from below by the mean size $S_f(f)$ of fragments that are newly formed, and from above by the mean size $S_m(f)$ of fragments that become mobilized and begin to migrate. The mean values were defined as $S(f) = \sum s^2 N_s(f) / \sum s N_s(f)$, where $N_s(f)$ is the number density of fragments of size s at gradient f. At low f, S_f fluctuates due to poor statistics.

The experiment presented here deals with the migration of a fractal fluid cluster of macroscopic size through a disordered medium. The migration is driven by a continuously increasing buouyancy force. In the course of the

migration process, the original cluster disintegrates and fragments are formed. The fragment size distributions appear curved on a log-log scale, giving no convincing evidence for a power law. The process may be modeled with good qualitative and quantitative agreement using a modified site-bond IP model. The dynamics exhibited by the migration process calls for further exploration.

We thank A. Aharony, K. Christensen, V. Frette, P. King, R. Lenormand, and K. J. Måløy for helpful discussions. We gratefully acknowledge support by VISTA, a research cooperation between the Norwegian Academy of Science and Letters and Den norske stats oljeselskap a.s. (STATOIL) and by NFR, the Norwegian Research Council.

[1] M.F. Gyure and B.F. Edwards, Phys. Rev. Lett. **68**, 2692 (1992).
[2] J.F. Gouyet, Phys. Rev. B **47**, 5446 (1993).
[3] R. Lenormand and S. Bories, C. R. Acad. Sci. **291**, 279 (1980); R. Chandler, J. Koplik, K. Lerman, and J.F. Willemsen, J. Fluid Mech. **119**, 249 (1982); D. Wilkinson and J.F. Willemsen, J. Phys. A **16**, 3365 (1983).
[4] R. Lenormand, C. Zarcone, and A. Sarr, J. Fluid Mech. **135**, 337 (1983).
[5] J.D. Chen and J. Koplik, J. Coll. Int. Sci **108**, 304 (1985).
[6] N.C. Wardlaw and Y. Li, Trans. Porous Media **3**, 17 (1988).
[7] D. Wilkinson, Phys. Rev. A **30**, 520 (1984); **34**, 1380 (1986).
[8] E. Clément, C. Baudet, and J. P. Hulin. J. Phys. Lett. (Paris) **46**, L1163 (1985); E. Clément, C. Baudet, E. Guyon, and J.P. Hulin, J. Phys. D **20**, 608 (1987).
[9] A. Birovljev, L. Furuberg, J. Feder, T. Jøssang, K. J. Måløy, and A. Aharony, Phys. Rev. Lett. **67**, 584 (1991).
[10] V. Frette, J. Feder, T. Jøssang, and Paul Meakin, Phys. Rev. Lett. **68**, 3164 (1992).
[11] P. Meakin, J. Feder, V. Frette, and T. Jøssang, Phys. Rev. A **46**, 3357 (1992).
[12] M. Blunt, M.J. King, and H. Scher, Phys. Rev. A **46**, 7680 (1992).
[13] P. Meakin, G. Wagner, J. Feder, and T. Jøssang, Physica A **200**, 241 (1993).
[14] G. Wagner, A. Birovljev, P. Meakin, J. Feder, and T. Jøssang (unpublished).

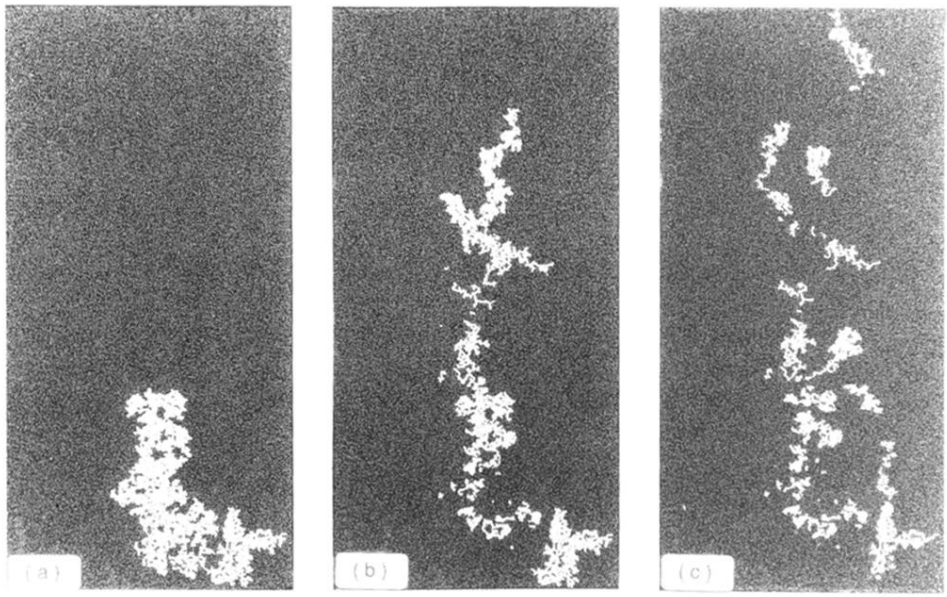

FIG. 1. (a)–(c) Pattern observed at $\theta = 0°$, 14°, and 53°, respectively. The original IP cluster shown in white covered approximately 2000 pores. (d)–(f) Simulated migrating IP clusters at $f = 0$, 0.005, and 0.013, respectively.

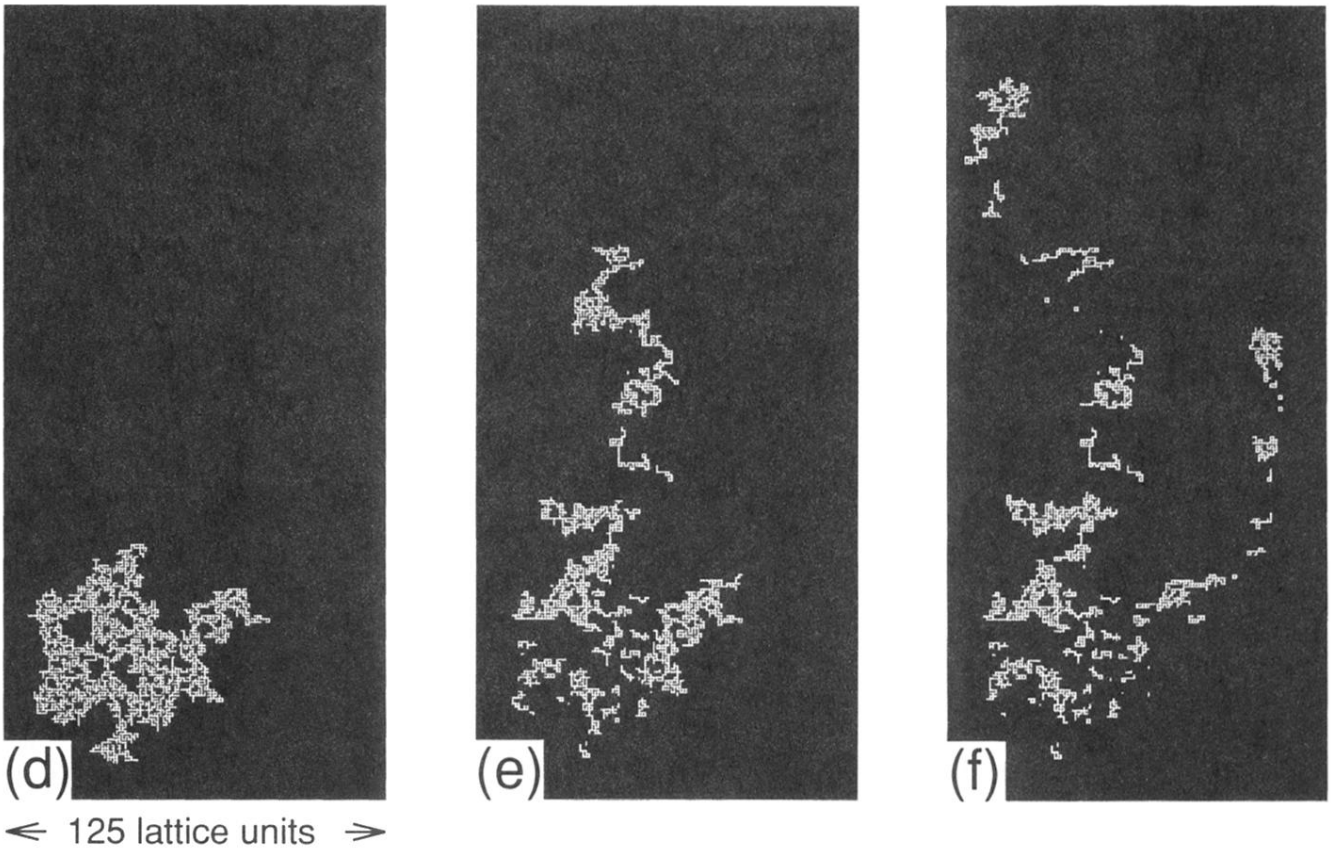

FIG. 1 *(Continued).*